World Academy of Science, Engineering and Technology
International Journal of Geological and Environmental Engineering
Vol:18, No:2, 2024

Optimization of Shale Gas Production by Advanced Hydraulic Fracturing

Fazl Ullah, Rahmat Ullah

***Abstract*—**This paper shows a comprehensive learning focused on the optimization of gas production in shale gas reservoirs through hydraulic fracturing. Shale gas has emerged as an important unconventional vigor resource, necessitating innovative techniques to enhance its extraction. The key objective of this study is to examine the influence of fracture parameters on reservoir productivity and formulate strategies for production optimization. A sophisticated model integrating gas flow dynamics and real stress considerations is developed for hydraulic fracturing in multi-stage shale gas reservoirs. This model encompasses distinct zones: a single-porosity medium region, a dual-porosity average region, and a hydraulic fracture region. The apparent permeability of the matrix and fracture system is modeled using principles like effective stress mechanics, porous elastic medium theory, fractal dimension evolution, and fluid transport apparatuses. The developed model is then validated using field data from the Barnett and Marcellus formations, enhancing its reliability and accuracy. By solving the partial differential equation by means of COMSOL software, the research yields valuable insights into optimal fracture parameters. The findings reveal the influence of fracture length, diversion capacity, and width on gas production. For reservoirs with higher permeability, extending hydraulic fracture lengths proves beneficial, while complex fracture geometries offer potential for low-permeability reservoirs. Overall, this study contributes to a deeper understanding of hydraulic cracking dynamics in shale gas reservoirs and provides essential guidance for optimizing gas production. The research findings are instrumental for energy industry professionals, researchers, and policymakers alike, shaping the future of sustainable energy extraction from unconventional resources.

***Keywords*—**Fluid-solid coupling, apparent permeability, shale gas reservoir, fracture property, numerical simulation.

I. Introduction

THE growing global demand for energy, coupled with the depletion of conventional hydrocarbon reserves, has led to an increased focus on unconventional energy sources. Among these, shale gas has emerged as a significant and promising resource, revolutionizing the energy landscape. Shale gas reservoirs, categorized by their low permeability and intricate geological formations, necessitate innovative techniques to enhance production [1].

Hydraulic fracturing, commonly known as "fracking," has become a pivotal technology in unlocking the vast potential of shale gas tanks. This process involves the injection of high-pressure liquid into the reservoir rock to make fractures, thereby increasing the pathways for gas to flow and improving overall production rates [2]. However, effective production optimization through hydraulic fracturing involves a complex interplay of various parameters, such as fracture design, reservoir properties, and operational strategies [3].

The challenge lies in striking a balance between maximizing gas recovery and minimizing operational costs while ensuring sustainable and environmentally responsible extraction. As such, extensive research efforts have been dedicated to understanding the intricate mechanisms that govern gas flow, rock deformation, fluid interactions, and fracture behavior within shale formations [4].

Shale gas manufacture is directly wedged by fracture factors, and the severities of these impacts vary with parameters. To assess the inspiration of parameters related to fractures on reservoir productivity, a discrete fracture system model was formulated. A triple-continuum classical was developed by He [5] to examine the connection between kerogens and production. Additionally, the effect of fracture diversion loss on increasing manufacture was examined using a completely coupled flow deformation model [6]. Additionally, Wang et al. [7] developed a two-phase flow-back model in order to examine how fracture factors affect production rate. All of these studies examined the connection between fracture features and production, but they stopped short of examining the effects of individual fracture features on gas yield. As a result, this study examines the fracture characteristics and statistically compares how they affect gas production.

The two primary techniques for handling hydraulic fractures in the reservoir arithmetical modeling are separate fracture model and entrenched distinct fractures models (EDFM). Distinct Fracture Model (DFM) meshes the surrounding matrix rock to match the fracture and displays fractures as explicit features [8], [9]. Since the fracture meshing is detached using EDFM, high-quality unstructured grids are not required [10]. Without taking into account the propagation of fractures, EDFM and DFM could successfully describe the complicated fracture geometry and carry out pool numerical modeling. In other words, their study treats fracture propagation in addition reservoir numerical imitation as two separate courses. In actuality, the two processes ought to function as a whole [11]. Recent papers [27], [28] have attempted to resolve this problem by modeling these two procedures in order.

Tomac & Gutierrez [12] utilized Uniform Fracture Model (UFM) to produce intricate hydraulic break geometry. Subsequently, they conducted reservoir arithmetical simulation to assess the increase in shale gas production after meshing the fractures using an unstructured grid. In order to determine production performance, Yu et al. [13] first replicated fracture proliferation through DDM and then pragmatic fractures

Fazl Ullah Brains Institute Peshawar, KPK, Pakistan (phone: +92-341-9391379; e-mail: fazlullah0341@gmail.com).

Rahmat Ullah Brains Institute Peshawar, KPK, Pakistan (phone: +92-340-9499819; e-mail: rahmatullahyousafzai@gmail.com).

geometry to a semi-analytical model. In order to model the manufacture of tight oil, Xu et al. [14] employed Capillary Zone Model (CZM) to simulate break spread and generate intricate geometric patterns. They then applied the intricate breaks to EDFM. The impact of mechanical rock qualities and stress regime was investigated. However, achievement quality, which are thought to control hydraulic break growing and have a substantial impact on well productivity, are not taken into account by these techniques. Ibrahim and Salah [15] suggested a comprehensive plan that considers both the stress public and conclusion quality into account, but pool heterogeneity—which is regarded as one of the major influences affecting productivity [16], [17], has not been quantitatively described.

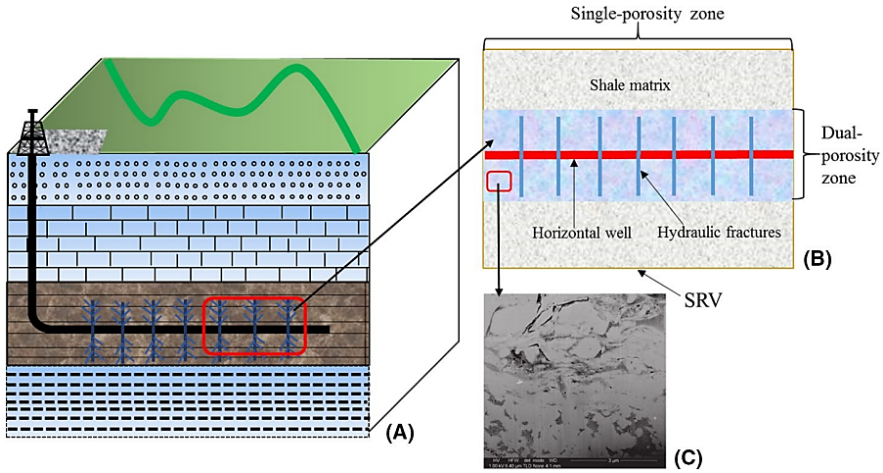

Fig. 1 (A) Illustration of the multistage hydraulic cracking method used in reservoirs of shale gas, (B) 2-D figure of a flat well with multiple stages of fracture, and, (C) Image from scanning electron microscopy

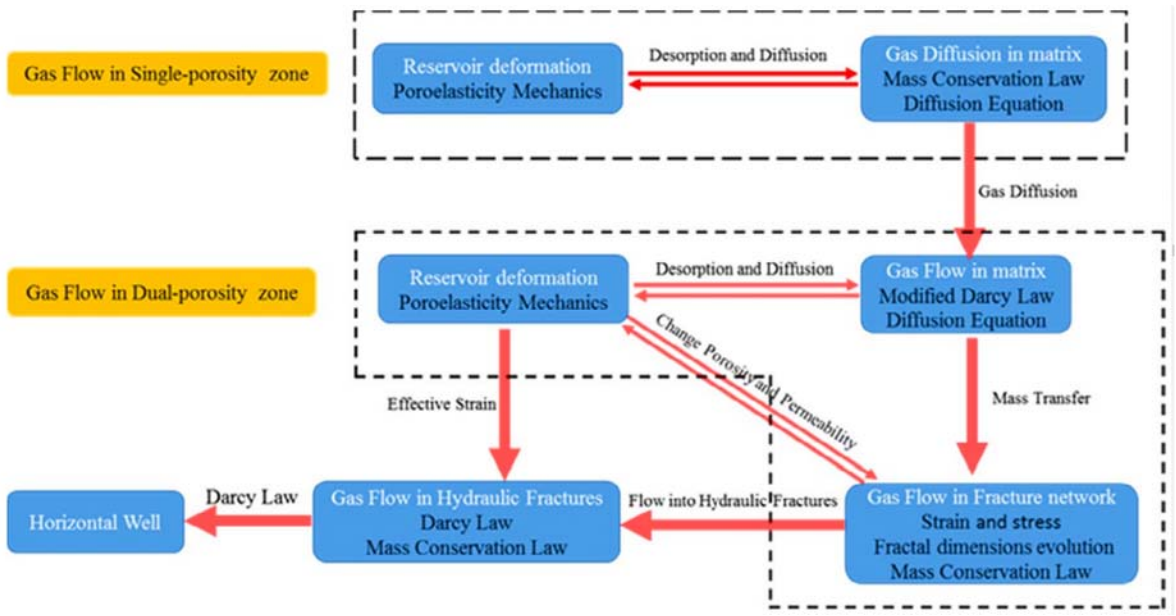

Fig. 2 The correlation exists between the deformation of shale and the flow of gas in regions characterized by multiple scales

II. The Equation Governing Gas Flow

Two segments of the shale gas reservoir, each characterized by distinct gas flow and solid deformation mechanisms within the shale medium, were isolated. Each zone's diffusion and deformation details are shown in Fig. 2. The following model describes their governing equations.

A. Equation Controlling a Single Porosity Medium

Shale gas's mass conservation equation is written as:

$$\frac{\partial(m_k)}{\partial t} + \nabla \cdot \left(-\frac{k_k}{\mu}\rho_{gk}\nabla p_k\right) = 0 \quad (1)$$

The expression for m_k represents the combined mass of gas, encompassing both adsorbed gases and free gas is stated as:

$$m_k = \rho_{gk}\phi_k + \rho_{ga}\rho_s\frac{V_L p_k}{p_k + p_L} \quad (2)$$

In (2), the symbol ρ_{gk} represents the density of the gas, while

ρ_{ga} pertains to the density of the gas under standard conditions. Additionally, ρ_s stands for the concentration of the V_L and shale matrix, corresponds to the constant Langmuir size. As per the ideal gases law, the gas mass can be well-defined as follows:

$$\rho = \frac{pM_g}{ZRT} \tag{3}$$

The compression coefficient, denoted as Z, is raised to the power of 27/49. This exponent can be approximated using the developmental correlation that relates the pseudo-reduced pressure (p_r) to the pseudo-reduced temperature (T_r).

$$Z = 0.702e^{-2.5Tr}p_r^2 - 5.524e^{-2.5Tr}p_r + (0.044T_r^2 - 0.164T_r + 1.15) \tag{4}$$

In the context of this equation, p_r represents the proportion of pressure (p) to the critical pressure p_c, and T_r represents the proportion of temperature (T) to the critical temperature T_c of methane. In (5), correlation provided can be used to determine gas viscosity:

$$\begin{cases} \xi = \frac{(9.379+0.01607M_g)(1.8T)^{1.5}}{209.2+19.26M_g+1.8T} \\ X = 3.448 + \frac{986.4}{1.8T} + 0.01009M_g \\ Y = 2.447 - 0.2224X \\ \mu = (1\times 10^{-7})\xi \exp\left(X(10^{-6}\rho)^Y\right) \end{cases} \tag{5}$$

Considering the notable impact of effective stress and apparent permeability of gas flow state, the expression for dynamic porosity can be formulated as follows, where ϕ_k represents the absorbency of the single-porosity region.

$$\phi_k = \phi_{k0}\exp\left[-C_m\left(\bar{\sigma} - \bar{\sigma}_0 - (P_k - P_0)\right)\right] \tag{6}$$

By inserting (5) into (6), we derive the principal equation governing the flow of gas within the shale matrix:

$$\left(\phi_k + p_a\rho_s\frac{V_L p_L}{(p_k+p_L)^2}\right)\frac{\partial p_k}{\partial t} + p_k\frac{\partial \phi_k}{\partial t} + \nabla\cdot\left(-\frac{k_k}{\mu}p_k\nabla p_k\right) = 0 \tag{7}$$

B. Governing Equation of Dual Porosity Medium

The equations governing mass preservation for gas flow within a matrix and brake system are as follows:

$$\begin{cases} \frac{\partial m_m}{\partial t} + \nabla\cdot\left(-\rho_m\frac{k_m}{\mu}\nabla p_m\right) = q_m \\ \frac{\partial m_f}{\partial t} + \nabla\cdot\left(-\rho_f\frac{k_f}{\mu}\nabla p_f\right) = -q_m \end{cases} \tag{8}$$

In the given context, μ represents the dynamic viscidness of the gas, while ρ_m and ρ_f denote the densities of the crack and medium of shale gas reservoir, correspondingly. The term q_m signifies the gas sink or source, and t denotes time [19]. Typically, the storage capacity and flow pathway for shale gases are represented by the fractures and mineral matrix, correspondingly. Here, m_m represents the gases mass within the shale matrix, encompassing together free and adsorbe gas, while m_f refers to the "mass of free" gases within the cracks, given the negligible contribution of further gases.

$$\begin{cases} m_m = \rho_m\phi_m + \rho_{ga}\rho_s\frac{V_L p_m}{p_m+p_L} \\ m_f = \rho_f\phi_f \end{cases} \tag{9}$$

The term on the right side of (9) serves as the sink or source of gas. This signifies that the gas dispersion procedure shifts from the pore structure to the matrix method [18]:

$$q_m = -\frac{\pi^2\rho_m k_m}{\mu}\left(\frac{1}{L_x^2} + \frac{1}{L_y^2}\right)(p_f - p_m) \tag{10}$$

Here, L_x and L_y represent the fracture displacement volumes in the x as well as y directions, correspondingly. As a consequence, the equations of partial differential central the fracture and matrix systems within (10) are as follows:

$$\begin{cases} \rho_m\left[\begin{matrix}\left(\frac{\phi_m}{p_m} + \frac{\rho_{ga}p_a}{p_m}\frac{V_L p_L}{(p_m+p_L)^2}\right) \\ -\phi_m c_m\left(\beta_m\frac{1-2v}{3} - 1 + \frac{E\varepsilon_L p_L}{9(p_m+p_L)^2}\right)\end{matrix}\right]\frac{\partial p_f}{\partial t} - \nabla\cdot\left(p_f\frac{k_f}{\mu}\nabla p_f\right) = \frac{\pi^2\rho_m k_m}{\mu}\left(\frac{1}{L_x} + \frac{1}{L_y}\right)(p_m - p_f) \\ \left[\phi_f + p_f\beta_f\left(1 - \frac{E}{E_S}\right)\frac{(1-2v)(1+v)}{E(1-v)}\right]\frac{\partial p_f}{\partial t} - \nabla\cdot\left(p_f\frac{k_f}{\mu}\nabla p_f\right) = \frac{\pi^2\rho_m k_m}{\mu}\left(\frac{1}{L_x} + \frac{1}{L_y}\right)(p_m - p_f) \end{cases} \tag{11}$$

C. Governing Equations the Flow of Gas in Hydraulic Fracture

As the pressure at the lowest hole decreases, shale gas migrates towards the internal border of the reservoir, which constitutes the system of hydraulic fracture. As an outcome, the fluid enters the lower orifice while adhering to the tangential trajectory of the crack. The flow of gas inside the hydraulic fracture adheres to Darcy's law [20]. The form conservation reckoning for the compressed fluid can be mathematically represented within this fracture system as follows:

$$d_f\frac{\partial(\rho_g\phi_{hf})}{\partial t} + \nabla_T\cdot\left(\rho_g q_{hf}\right) = 0 \tag{12}$$

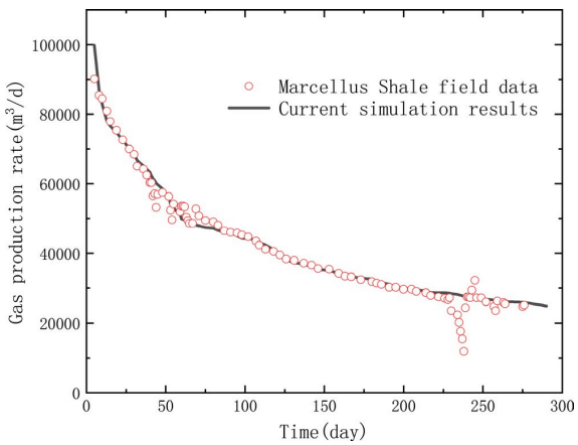

Fig. 3 Analyzing the Marcellus shale involves a comparison between simulation results and field data [21]

Here, d_{hf} represents the hydraulic fracture width, and χhf signifies the absorbency. The speed at the fracture border can be determined using Darcy's law:

$$q_{hf} = -d_{hf}\frac{k_{hf}}{\mu}\nabla_T p_{hf} \quad (13)$$

In this context, d_{hf} stands for the hydraulic fracture width, and p_{hf} represents the initial burden of the shale reservoir. As the fracturing process continues, the gas pressure within the reservoir gradually decreases, leading to a reduction in the effective penetrability within the secondary fractures [22]. This reduction is associated with the gas pressure and can be described as follows:

$$k_{hf} = k_{hf0}\exp\left(-c_f(p_{hf0} - p_{hf})\right) \quad (14)$$

The pressure-sensitive coefficient, denoted as cf, represents the hydraulic fractures on early permeability. The breakage's gas perviousness is notably elevated, resulting in a minor impact on the flow pattern. This observation underscores the significance of effective stress as a pivotal factor in gas production.

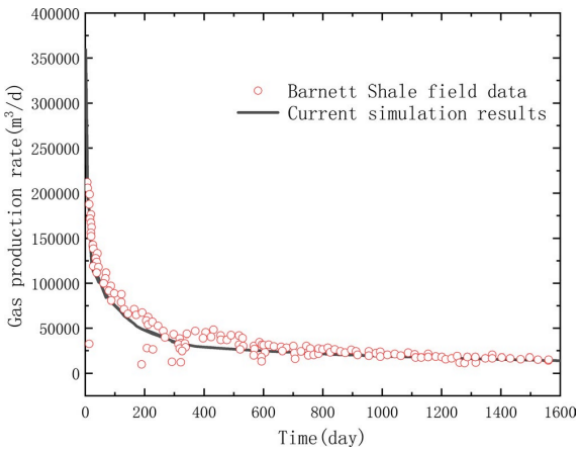

Fig. 4 Relationship of imitation results and field data of the Barnett shale

III. Model Verifications

By comparison the replication results with actual field information on the Marcellus and Barnett shale's gas output, we were able to validate the model. To test the model's accuracy in short-term production, the Marcellus shale's 300-day production data were used, and the Barnett shale's 4-year production data were used to test the accuracy of the model in long-term manufacture. The COMSOL Multiphysics was used to implement and resolve the governing calculations [23]. The solid mechanism module solves the motorized equilibrium equation of the shale gas tank, and the PDE module solves the gas flow problem. The consequences of the numerical imitation are essentially similar with the field data, as shown in Figs. 3 and 4. The free gas from the tank cracks flows quickly toward horizontal wells in the initial phases of shale gas production, causing a fast reduction in gas manufacture from the peak to the trough. The majority of the production in the later phase came from the matrix's adsorbed gas, and because the gas' desorption and dispersion processes were sluggish and prolonged, this stage's output gradually decreased.

IV. Results and Discussion

In order to assess the impact of critical fracture parameters on the extended-term gas extraction through multi-stage hydraulic fracturing, we established an integrated model that combines gas flow dynamics with real stress conditions in shale gas formations [24]. The first geometric representation seen in Fig. 5, commonly known as the "first geometric model," is the fundamental framework for our inquiry. This work has taken into account important geometric aspects in hydraulic fractures, such as the half-length, fracture width, and changing size, as well as the initial permeability and opening of natural fractures.

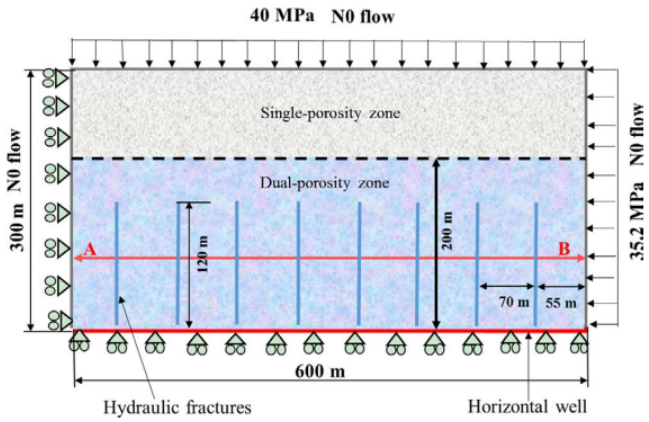

Fig. 5 Drawing of the 1st geometrical model (model 1)

In the initial geometric representation (Fig. 9), the modeled expanse gets partitioned into three distinct regions: a solitary-porosity medium section (100 m in vertical extent), a biporous medium section (200 m in vertical extent), and the hydraulic fracture section (indicated by the red stripe at the lowermost part of Fig. 9). In this depiction, the modeled expanse measures length 600 m and width 300 m. There are eight hydraulic fractures totaling 120 m in length, with a spacing of 70 m separating the next cracks. Around the boundary of the model, there is no gas flow. Pw is the bottom-hole pressure. The right border has a minimum pressure of 35.2 MPa and the top boundary has a maximum pressure of 40 MPa. The left boundary and the lower boundary are where the axis support is placed.

Fig. 6 demonstrates the first geometric model's reservoir pressure distribution at various stages of investigation. With the passing of time throughout production, the pressure scope keeps growing. The daily gas output reaches its peak after a year of production when the heaviness in the fracture equals the pressure in the bottom of the well. The diffusion mechanism causes the gas in the tank to be engrossed into the hydraulic crack. The pressure dispersal did not fluctuate much from year to year in the years that followed, showing that gas exploitation has peaked.

Fig. 7 demonstrates the reservoir pressure profile along the initial geometric model's cutting line A-B across various exploration times. At first, the gas pressure is very high, but it

gradually drops until it equals the pressure in the bottom of the well. Additionally, the pressure near the hydraulic fracture quickly decreases, demonstrating the hydraulic fracture's excellent ability to boost reservoir performance.

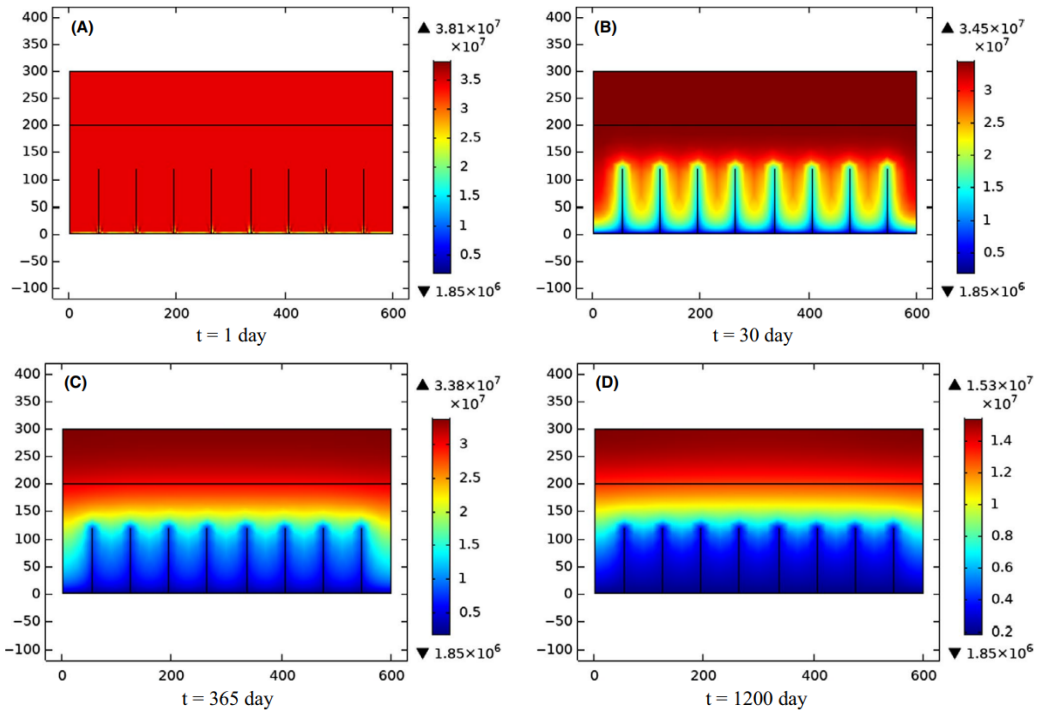

Fig. 6 Gas pressure distributions achieved using the initial geometric model at various time scales

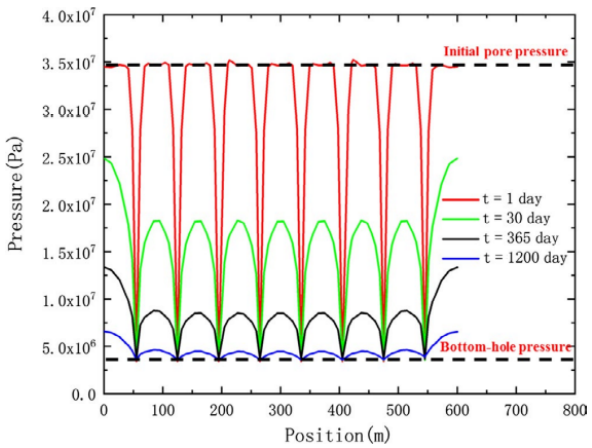

Fig. 7 Gas pressure outline alongside the line A-B within the 1st geometric model at diverse period intervals

A. Impact of the Geometric Parameters of Hydraulic Fractures

We created two additional geometric models, denoted to as second model and third model, in order to investigate the influence of hydraulic crack geometry on gas production. The breaks in the second model, depicted in Fig. 10 A, maintain the same geometric shape as those in the initial model (Fig. 5), but with varying lengths ranging between 80 m and 120 m. In the case of model 3 (Fig. 10 B), the main hydraulic fracture retains a length of 120 m, matching that of the first model [26]. However, this model incorporates multiple secondary fracture networks that align with the intricate fracture system found in real-world scenarios. The measurement of the eight primary hydraulic breaks is the same in all three geometric replicas [25].

Fig. 9 displays the increasing ratio of three geometric models on the production of shale gas. The third model produces the most gas. In comparison to the first model, the second model produced more gas. Despite having the same overall length, hydraulic fractures have a larger contact surface in the three-dimensional domain, the larger they are. Due to this, longer hydraulic cracks produce gas at a higher rate. The third models have a better fracture diversion capability since the hydraulic fissures are lengthier than in another typical. The original fractures are the same length overall, but numerous secondary hydraulic fractures increase the capacity of the fractures' diversion, resulting in a larger treatment area between neighboring fractures. In order to increase the efficiency of gas production, it is therefore useful to exploit the wider fracture diversion capacity that is brought about by the longer hydraulic fractures, which covers a larger action area.

B. Effect of Fracture Half-Length

We used the fracture half-lengths of 80 m, 40 m, 120 m, and 160 m to replicate the active fluctuations of the horizontal well creation, as revealed in Numeral 14. Gas production increases as the crack half-length increases, demonstrating a positive correlation between the two. The cumulative gas output over 1200 days is 6.49 × 107 m^3, 7.01 × 107 m^3, 6.69 × 107 m^3, and 7.56 × 107 m^3 for the half-lengths of 80 m, 120 m, 40 m, and 160 m, respectively. Consequently, lengthening hydraulic

fractures is one of the greatest efficient methods to increase shale gas reservoir production.

C. Effect of Fracture Width

The hydraulic breakage width is another crucial factor influencing the shale gas output [27]. The connection between hydraulic fracture width and shale gas manufacture is simulated in Fig. 9. The daily gas production initially drops off quickly before ultimately stabilizing. The primary cause is that large aperture fracture boosts production because it has high conductivity quickly. For stable gas production, the hydraulic fracture's width should be kept to a maximum of 0.003 meters.

D. Effect of Fracture Diversion Capacity

The fracture diversion volume is the amount of fluid supply that the supporting fracture can give [28]. Fig. 11 depicts our simulation of the gas output from horizontal wells through hydraulic fracture alteration capacities of 0.3 cm, 0.6 cm, 0.9 cm, and 1.2 cm.

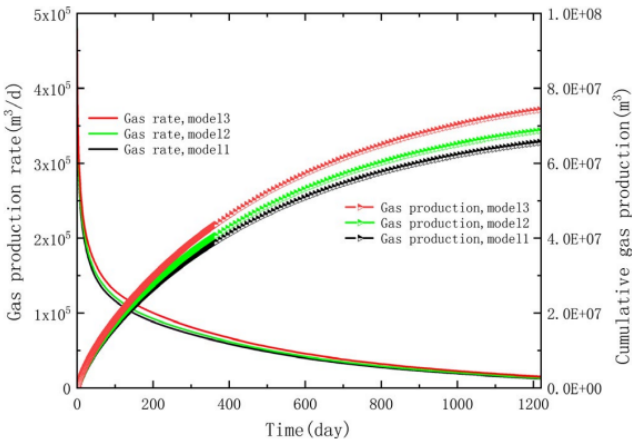

Fig. 8 Association between the gas production and hydraulic fracture uniformity

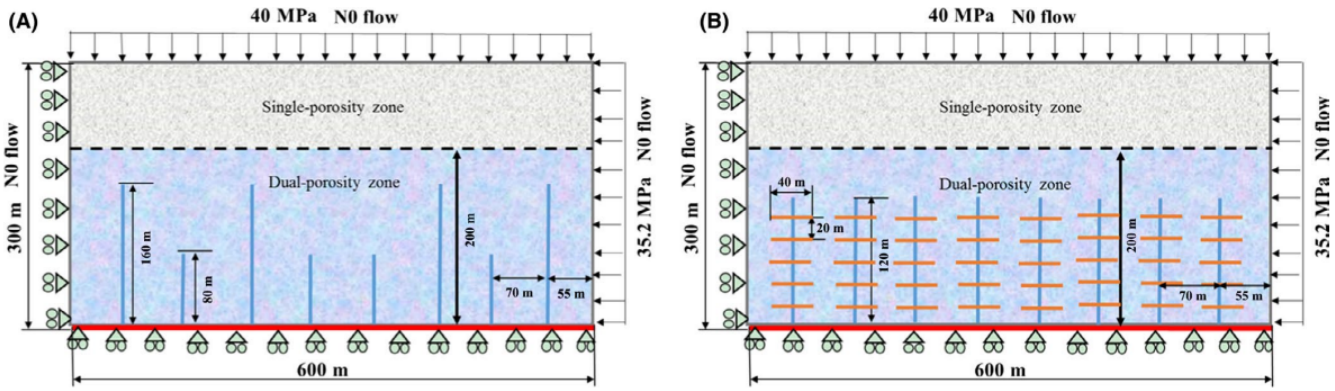

Fig. 9 The 2nd and 3rd geometric model

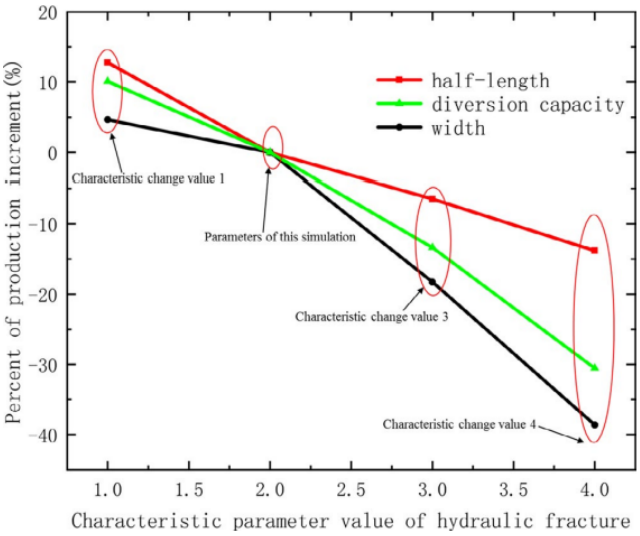

Fig. 10 The increase in production resulting from modifications in fracture structures

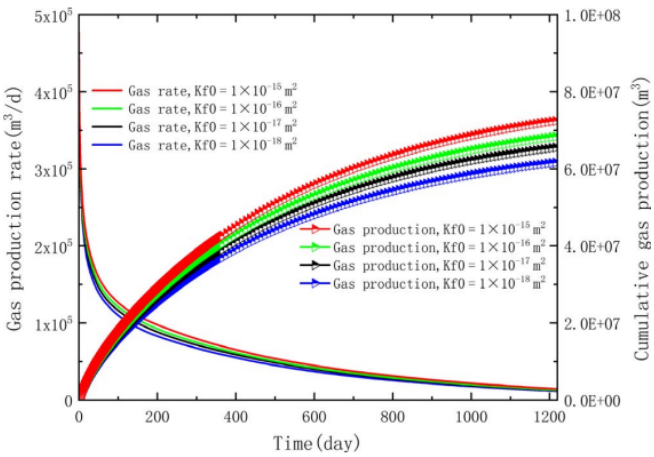

Fig. 11 Relationship among gas output and the initial natural break permeability (kf0)

After 1200 days, the increasing gas production for the four hydraulic fracture diversion capacities is 5.88 × 107 m^3, 7.31 × 107 m^3, 6.65 × 107 m^3, and 7.53 × 107 m^3. It demonstrates that increasing fracture conduction can boost shale gas production, but the rate of development is often modest, suggesting that the

fracture diversion capacity has been reached [29]. This is so that the varying diversion capacities of fractures will not affect the overall volume of gas in the pool, which is continual under the current circumstances. As a result, as the development progresses into a later phase, its production becomes gradually constant.

E. Effect of Natural Fracture

The initial natural penetrability and natural fracture opening of the usual fractures, as well as their effects on gas production, were also examined [30]. Fig. 12 illustrates how shale gas output rises as natural fracture permeability rises. It is evident that an appropriate initial porosity value leads to higher gas production, while an excessively high permeability value does not significantly enhance production. Shale gas production tends to stabilize when the permeability value exceeds 1 × 1016 m². Fig. 13 depicts the results of our analysis of the connection between natural fracture inaugural and gas production.

TABLE I
FACTORS INDUCING YIELD TEST

Parameter level	Number of models	Kf0/m^2	b0/m
1	3	1×10^{-15}	1×10^{-5}
2		1×10^{-16}	1×10^{-6}
3		1×10^{-17}	1×10^{-7}
4		1×10^{-18}	1×10^{-8}

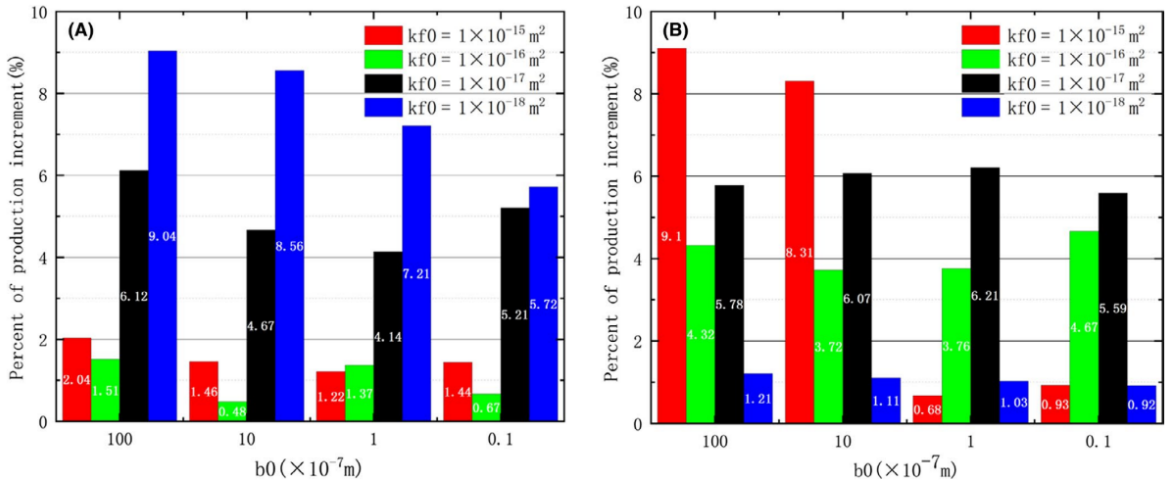

Fig. 12 Percentage of the growth in the creation of geometric models: (A) the increase in output from the 2nd model relative to the 1st model; (B), the increase in output from the third model relative to the first model

Production and the natural fracture opening are positively associated, which obviously affects production. For instance, after 600 days, the cumulative production from a fracture opening of 1 × 106 m is 5.58 × 107 m^3, whereas a fracture opening of 1 × 105 m is 6.20 × 107 m^3. There are several restrictions on this study, and the analysis above only takes into account the impact of one component on the outcome. Consequently, we employed the orthogonal experimental design system to examine the horizontal wells cumulative production across diverse groupings of parameters. This approach allowed us to assess the individual significance of every factor on production and determine the optimal set of fracture parameters by analyzing variations in initial porosity and the aperture of natural fractures.

We contrasted the three geometric models' contributions to gas manufacture. The opening and initial permeability of the three models' natural cracks vary. Fig. 13 A displays the 1200 days of production that the first and second versions brought. Due to the second model's improved reservoir storage, its production is 7.21% higher than that of the first model. It demonstrates that the second model can be used with shale gas reservoirs of low quality, such as those with usual fracture openings of 1 × 107 m and starting permeabilities of 1 × 1018 m^2. The production of the third model over 1200 days is higher than that of the initial model, as shown in Fig. 13 B. Therefore, lengthening the hydraulic fracture can significantly boost output for shale gas resources with high penetrability and well-developed fractures.

V. CONCLUSION

This study recognized a comprehensive and integrated classical for gas flow and stress conditions within shale gas reservoirs, encompassing hydraulic fracture zones, dual-porosity medium zones, and single-porosity medium zones. Within each zone, various aspects such as reservoir deformation, multiscale gas adsorption, surface diffusion, and flow were thoroughly examined. A model for apparent permeability within the medium and fracture system was developed, effectively capturing the real-state characteristics of a shale gas pool. This model was grounded in the principles of permeable elastic mediums, Darcy's law, fractal dimension evolution, and the law of mass conservation. The three zones model was used to describe how important fracture factors affect both rapid- and long-term shale gas recoveries.

The main variables determining the output of shale gas reservoirs are the associated hydraulic fracture characteristics. By comparation the increasing manufacture growth charges of the strictures, it is discovered that growing the hydraulic

breakage half-length, followed by increasing the fracture diversion capacity and width, results in the maximum increase of shale vapor production. Additionally, the shale gas production is meaningly impacted by natural fractures. Wider openings and increased fracture permeability support high production. We can also alter the shape of the hydraulic fracture in instruction to increase the manufacture of shale gas tank. While longer hydraulic fractures can result in higher output for reservoirs with massive fractures and comparatively high permeability, more compound shapes of hydraulic breaks can do the same for reservoirs with micro fractures and low permeability.

References

[1] Kreps BH. The rising costs of fossil-fuel extraction: an energy crisis that will not go away. American journal of economics and sociology. 2020 May;79(3):695-717.

[2] Badjadi MA, Zhu H, Zhang C, Naseem MH. Enhancing Water Management in Shale Gas Extraction through Rectangular Pulse Hydraulic Fracturing. Sustainability. 2023 Jul 10;15(14):10795.

[3] Suppachoknirun, T., & Tutuncu, A. N. (2017). Hydraulic fracturing and production optimization in Eagle Ford shale using coupled geomechanics and fluid flow model. Rock Mechanics and Rock Engineering, 50, 3361-3378.

[4] Eyinla DS, Leggett S, Badrouchi F, Emadi H, Adamolekun OJ, Akinsanpe OT. A comprehensive review of the potential of rock properties alteration during CO2 injection for EOR and storage. Fuel. 2023 Dec 1;353:129219.

[1] He, X. (2022). Fluid Flow in Fractured Rocks: Analysis and Modeling (Doctoral dissertation).

[2] Fan X, Li G, Shah SN, Tian S, Sheng M. Analysis of a fully coupled gas flow and deformation process in fractured shale gas reservoirs. J Nat Gas Sci Eng. 2015;27:901-913.

[3] Wang JG, Liu J, Kabir A. Combined effects of directional compaction, non-Darcy flow and anisotropic swelling on coal seam gas extraction. Int J Coal Geol. 2013;109:1-14.

[4] Zhao Y, Jiang H, Rahman S, Yuan Y, Zhao L, Li J, Ge J, Li J. Three-dimensional representation of discrete fracture matrix model for fractured reservoirs. Journal of Petroleum Science and Engineering. 2019 Sep 1;180:886-900.

[5] Hui MH, Karimi-Fard M, Mallison B, Durlofsky LJ. A general modeling framework for simulating complex recovery processes in fractured reservoirs at different resolutions. SPE Journal. 2018 Apr 12;23(02):598-613.

[6] Olorode O, Wang B, Rashid HU. Three-dimensional projection-based embedded discrete-fracture model for compositional simulation of fractured reservoirs. SPE Journal. 2020 Aug 13;25(04):2143-61.

[7] Wang, J., Wei, Y., Pan, Y., & Yu, W.. Optimization Method for Fracture-Network Design Under Transient and Pseudosteady Condition Using UFD Technique and Deep Learning Approach. In SPE/AAPG/SEG Unconventional Resources Technology Conference (p. D031S075R002). 2023 June URTEC.

[8] Weng X, Kresse O, Chuprakov D, Cohen CE, Prioul R, Ganguly U. Applying complex fracture model and integrated workflow in unconventional reservoirs. Journal of Petroleum Science and Engineering. 2014 Dec 1;124:468-83.

[9] Yu W, Hu X, Wu K, Sepehrnoori K, Olson JE. Coupled fracture-propagation and semianalytical models to optimize shale gas production. SPE Reservoir Evaluation & Engineering. 2017 Nov 16;20(04):1004-19.

[10] Xu S, Feng Q, Li Y, Wang S. An integrated workflow for fracture propagation and reservoir simulation in tight oil. Journal of Petroleum Science and Engineering. 2019 Aug 1;179:1159-72.

[11] Salah M, Ibrahim M. Engineered fracture spacing staging and perforation cluster spacing optimization for multistage fracturing horizontal wells. InSPE annual technical conference and exhibition 2018 Sep 24. OnePetro.

[12] Tomac, I., & Gutierrez, M. (2020). Micromechanics of hydraulic fracturing and damage in rock based on DEM modeling. Granular Matter, 22, 1-17.

[13] Ghanizadeh A, Clarkson CR, Clarke KM, Yang Z, Rashidi B, Vahedian A, Song C, DeBuhr C, Haghshenas B, Ardakani OH, Sanei H. Effects of entrained hydrocarbon and organic-matter components on reservoir quality of organic-rich shales: implications for "sweet spot" identification and enhanced-oil-recovery applications in the Duvernay formation (Canada). SPE journal. 2020 Jun 11;25(03):1351-76.

[14] Lee AL, Gonzalez MH, Eakin BE. The viscosity of natural gases. J Petrol Technol. 1966;18(08):997-1000.

[15] Jin, H., Liu, C., Guo, Z., Zhang, Y., Niu, C., Wang, D., & Ling, Y. (2021). Rock physical modeling and seismic dispersion attribute inversion for the characterization of a tight gas sandstone reservoir. Frontiers in Earth Science, 9, 641651.

[16] Pogrebnyak, V. G., Chudyk, I. I., & Perkun, I. V. (2022). Solutions of polymers in the oil and gas technologies. Prospects for Developing Resource-Saving Technologies in Mineral Mining and Processing, 110.

[17] Arias Ortiz, D., Bounceur, N., & Patzek, T. W. (2022, September). Validation and Analysis of the Physics-Based Scaling Curve Method for Ultimate Recovery Prediction in Hy-Draulically Fractured Shale Gas Wells. In SPE Annual Technical Conference and Exhibition? (p. D031S060R003). SPE.

[18] Men, X., Tao, S., Liu, Z., Tian, W., & Chen, S. (2021). Experimental study on gas mass transfer process in a heterogeneous coal reservoir. Fuel Processing Technology, 216, 106779.

[19] Kong, B., Chen, S., Chen, Z., & Zhou, Q. (2020). Bayesian probabilistic dual-flow-regime decline curve analysis for complex production profile evaluation. Journal of Petroleum Science and Engineering, 195, 107623.

[20] Pearson, C. M., Fowler, G., Stribling, K. M., McChesney, J., McClure, M., McGuigan, T., ... & Wildt, P. (2020, October). Near-wellbore deposition of high conductivity proppant to improve effective fracture conductivity and productivity of horizontal well stimulations. In SPE Annual Technical Conference and Exhibition. OnePetro.

[21] Wang, W., & Taleghani, A. D. (2017). Impact of hydraulic fracturing on cement sheath integrity; A modelling approach. Journal of Natural Gas Science and Engineering, 44, 265-277.

[22] Aabø, T. M., Oldfield, S. J., Yuan, H., Kammann, J., Sørensen, E. V., Stemmerik, L., & Nielsen, L. (2023). Establishing a High Resolution 3D Fracture Dataset in Chalk: Possibilities and Obstacles Working with Outcrop Data. In Geomechanical Controls on Fracture Development in Chalk and Marl in the Danish North Sea: Understanding and Predicting Fracture Systems (pp. 9-46). Cham: Springer International Publishing.

[23] Quosay, A. A., Knez, D., & Ziaja, J. (2020). Hydraulic fracturing: New uncertainty based modeling approach for process design using Monte Carlo simulation technique. PLoS One, 15(7), e0236726.

[24] Lin, M., Chen, S., Ding, W., Chen, Z., & Xu, J. (2015). Effect of fracture geometry on well production in hydraulic-fractured tight oil reservoirs. Journal of Canadian Petroleum Technology, 54(03), 183-194.

[25] Tang, R., Xie, J., Xue, S., Zhang, Z., Liu, J., & Yang, B. (2022). Research on seepage characteristics of Y-shaped fractures under different fracture roughness. Geofluids, 2022.

[26] Zhao, H., Wu, K., Huang, Z., Xu, Z., Shi, H., & Wang, H. (2021). Numerical model of CO2 fracturing in naturally fractured reservoirs. Engineering Fracture Mechanics, 244, 107548.

[27] Xu, S., Guo, J., Feng, Q., Ren, G., Li, Y., & Wang, S. (2022). Optimization of hydraulic fracturing treatment parameters to maximize economic benefit in tight oil. Fuel, 329, 125329.

[28] Fu, S., Yu, J., Zhang, K., Liu, H., Ma, B., & Su, Y. (2020). Investigation of multistage hydraulic fracture optimization design methods in horizontal shale oil wells in the Ordos Basin. Geofluids, 2020, 1-17.